Corrections

PHYSICS. For the article "Organic light-emitting diodes formed by soft contact lamination," by Tae-Woo Lee, Jana Zaumseil, Zhenan Bao, Julia W. P. Hsu, and John A. Rogers, which appeared in issue 2, January 13, 2004, of *Proc. Natl. Acad. Sci. USA* (**101,** 429–433; first published January 2, 2004; 10.1073/pnas.0304179101), the authors note that on page 430, left column, 5 lines from the bottom, "electron beam with long distance (≈30 cm)" should read "electron beam with long distance (≈40 cm)." Also, due to a printer's error, the scale bar is missing from Fig. 4*a*, and Fig. 2*a* should have been labeled "Current density (mA/mm^2)" instead of "Current density (mA/MM^2)." The corrected figures and their legends appear below.

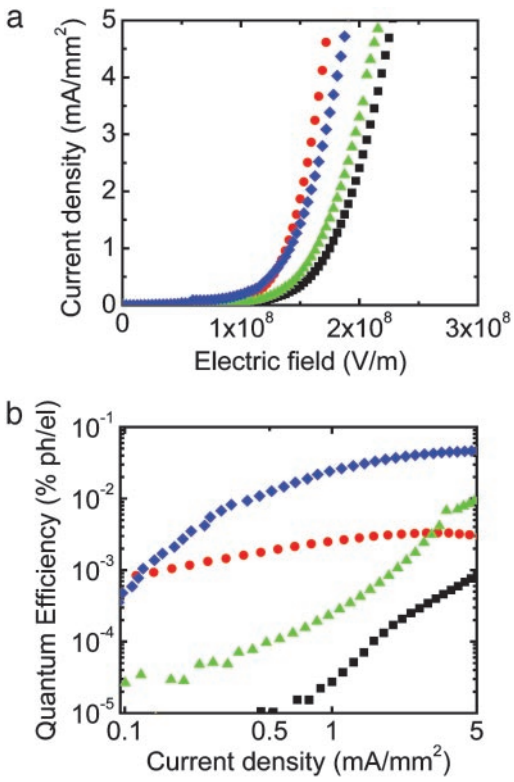

Fig. 2. Characteristics of OLEDs formed from a stack of ITO (100 nm)/MEH-PPV (65 nm)/Au (20 nm), fabricated by ScL and by evaporation (conventional) of the Au layer. (*a*) Current density as a function of electric field. (*b*) External quantum efficiency [% photons per electron (ph/el)] as a function of current density. Squares, conventional device operated with ITO positively biased; triangles, ScL device operated with ITO positively biased; circles, conventional device operated with Au positively biased; diamonds, ScL device with Au positively biased. For both bias directions, the efficiency of the ScL device is much higher than that of the conventional device

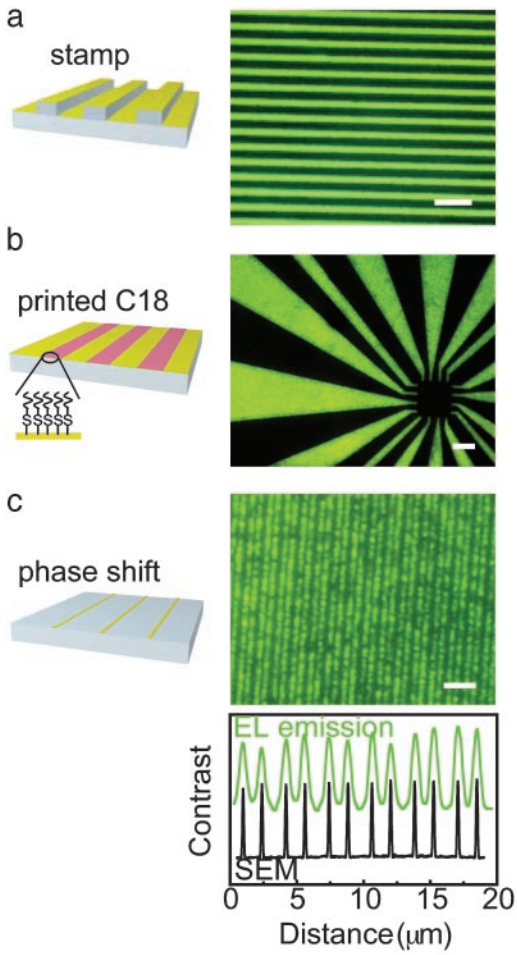

Fig. 4. Patterned OLEDs formed by the combined use of ScL and soft lithography. In all cases, the Au was 20 nm thick and the electroluminescent layer was a polyfluorene derivative blended with 17 wt % of $TBABF_4$ (100 nm). The unpatterned devices showed EL efficiencies of 0.65% ph/el. The schematic illustrations on the left show the modifications to the ScL electrodes, and the images on the right represent an example of OLEDs fabricated by using the approach. (*a*) Molding features of relief into the PDMS followed by blanket deposition of the electrode generates emission in the pattern of the raised features. (Scale bar, 100 μm.) (*b*) Microcontact printing an insulating self-assembled monolayer (octadecanethiol; C18) before lamination yields emission only in the bare Au regions. (Scale bar, 100 μm.) (*c*) Photolithography with a conformable phase mask followed by etching directly patterns lines (150 nm wide) of Au on the PDMS. The averaged linewidth (≈ 600 nm) of the pattern of emission (graph below) in this case is comparable to the resolution of the optical imaging system. (Scale bar, 5 μm.) The Rayleigh diffraction limit for the 0.55-numerical-aperture microscope objectives is 590 nm at a wavelength of 540 nm. The EL image was taken through the ITO (100 nm)/glass (0.4 mm), which reduces the effective numerical aperture.

www.pnas.org/cgi/doi/10.1073/pnas.0400055101

NEUROSCIENCE. For the article "A unifying basis of auditory thresholds based on temporal summation," by Peter Heil and Heinrich Neubauer, which appeared in issue 10, May 13, 2003, of *Proc. Natl. Acad. Sci. USA* (**100,** 6151–6156; first published April 30, 2003; 10.1073/pnas.1030017100), the authors note that when they recalculated absolute thresholds in μPa·s from measurements on goldfish published by Fay and Coombs [Fay, R. R. and Coombs, S. (1983) *Hearing Res.* **10,** 69–92], it escaped their attention that the dB values plotted in the paper were based on a reference pressure of 1 dyne/cm^2 rather than on 20 μPa. Thus, the real thresholds for the goldfish are higher than the ones plotted in black dots in Fig. 3*d* by a factor of 5,000. The authors point out that this error does not affect any of the conclusions, because it results only in an upward shift of the function for the goldfish in Fig. 3*d*. The slope *m* of this function also is unaffected by this difference in the reference pressure. The corrected figure and its legend appear below.

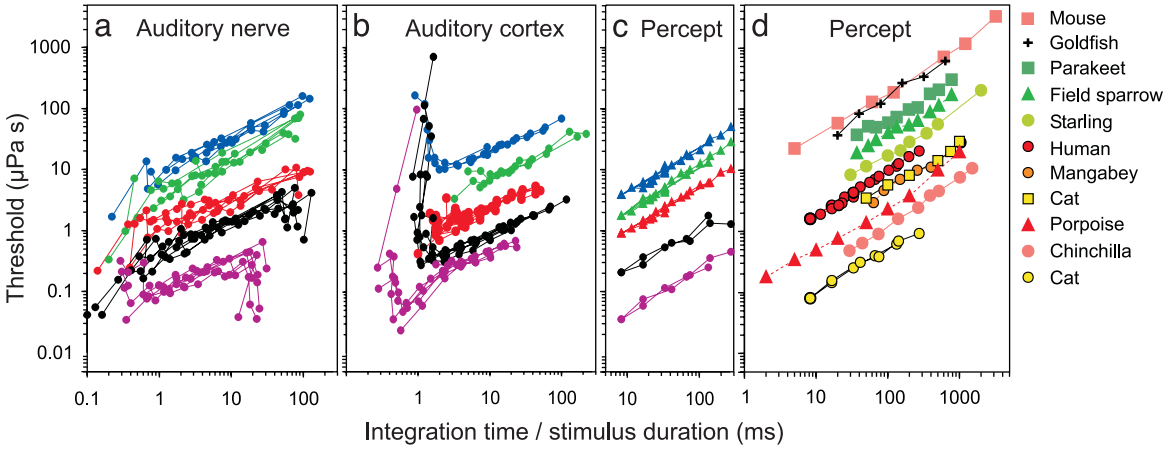

Fig. 3. Comparison of the pressure envelope integration thresholds for neuronal (*a* and *b*) and perceptual (*c* and *d*) measurements. Shown are plots of thresholds for 5 AN fibers (*a*) and 5 AI neurons (*b*) with different CFs (different colors). Lines connect thresholds derived from tones of different SPLs but of the same onset function and onset time. (*c*) Analogous functions for perceptual thresholds for two cats (purple and black circles) and three humans (red, green, and blue triangles). Lines connect thresholds obtained with stimuli of different series (see Fig. 2*a*). (*d*) Analogous functions for mean perceptual thresholds for a range of vertebrate species, calculated from published data (8–14, 17–19). For the porpoise, parakeet, and field sparrow, absolute thresholds could not be determined from the original articles and thus the position on the ordinate is arbitrary.

www.pnas.org/cgi/doi/10.1073/pnas.0308741101